

1 **Coupling of the VAMPER permafrost model within the earth system model iLOVECLIM** 2 **(version 1.0): description and validation**

3 D. Kitover, R. van Balen, D.M. Roche, J. Vandenberghe, H. Renssen

4 Earth and Climate Cluster, Faculty of Earth and Life Sciences, Vrije Universiteit Amsterdam, Amsterdam,
5 the Netherlands

6 Correspondence to: D.C. Kitover (d.c.kitover@vu.nl)

7 **Abstract**

8 The VAMPER permafrost model has been enhanced for coupling within the iLOVECLIM earth system
9 model of intermediate complexity by including snow thickness and active layer calculations. In addition,
10 the coupling between iLOVECLIM and the VAMPER model includes two spatially variable maps of
11 geothermal heat flux and generalized lithology. A semi-coupled version is validated using the modern
12 day extent of permafrost along with observed permafrost thickness and subsurface temperatures at
13 selected borehole sites. The modeling run not including the effects of snow cover overestimate the
14 present permafrost extent. However, when the snow component is included, the extent is overall
15 reduced too much. It was found that most of the modeled thickness values and subsurface
16 temperatures fall within a reasonable range of the corresponding observed values. Discrepancies are
17 due to lack of captured effects from features such as topography and organic soil layers. In addition,
18 some discrepancy is also due to disequilibrium with the current climate, meaning that some permafrost
19 is a result of colder states and therefore cannot be reproduced accurately with the iLOVECLIM
20 preindustrial forcings.

21

22 **1 Introduction**

23 The **VU Amsterdam Permafrost (VAMPER)** model is a deep 1-d heat conduction model with phase
24 change capability. At a number of arctic/subarctic locations, the model has simulated both equilibrium
25 and transient permafrost depth estimates (Kitover et al., 2012; Kitover et al., 2013). The model was built
26 with the intention to couple it within iLOVECLIM, an earth system model of intermediate complexity.
27 Although the VAMPER model simulations have been previously validated and forced using climate
28 model data, a common technique for modeling permafrost, the next step is to build on these
29 developments, providing the ability to investigate the permafrost-climate relationship. Therefore,
30 VAMPER has been enhanced so that it may be more realistically coupled within iLOVECLIM. With this
31 coupling, it is the ultimate goal to capture the transient nature of permafrost growth/decay over
32 millennia as a feedback effect during major periods of climate change. However, as a first step, the
33 VAMPER model has been semi-coupled to ECBilt, the atmospheric module that includes the land
34 component within iLOVECLIM, to validate the simulation of modern-day permafrost extent and
35 thickness. We use the term semi-coupled since the coupling is only one-directional (from ECBilt to
36 VAMPER). In other words, the effects of (changing) permafrost are not fed back to the climate.- The goal

1 of this paper is to describe this coupling and then analyze the validation experiment for modeling
2 present-day permafrost, with detailed explanation of why mismatches occur between simulated and
3 observed data.

4 The first example of VAMPER as a stand-alone deep permafrost model was for Barrow, Alaska (Kitover
5 et al., 2012) where the experiment simply reproduced the present-day permafrost depth using monthly
6 averaged observation data of ground "surface" (- 1 cm deep) temperatures. In this same study,
7 VAMPER was also validated by comparing results against other developed deep permafrost models (also
8 used for millennial-scale simulations) using similar forcings and parameter settings. In both Kitover et al.
9 (2012) and Kitover et al. (2013), a number of transient simulations at selected locations (e.g. Wyoming,
10 West Siberia, Central Siberia) were performed using the stand-alone version of the VAMPER model,
11 forced by *i*LOVECLIM-generated air surface temperatures over the last 21k years (Roche et al., 2011). In
12 addition, a sensitivity analysis was presented in Kitover et al. (2013), showing the range of simulated
13 permafrost depths under different parameter settings.

14 Thus far, according to the work summarized above, VAMPER has only been employed as a post-
15 processing, site-specific permafrost model. However, the advantage of the model being simple with
16 limited parameterization requirements, hence resulting in speedy computation times, have not been
17 fully realized since it is not yet coupled within *i*LOVECLIM. As a next step, this paper describes the
18 necessary developments to couple VAMPER with ECBilt, the atmospheric component of *i*LOVECLIM, via
19 the air surface temperature. Specifically, this presented work introduces two enhancements to the
20 VAMPER model : 1) inclusion of ~~a~~-snow as optional layers and 2) change in the timestep. The first in
21 particular is a common issue in modeling permafrost since snow cover is a widely recognized influence
22 on the ground thermal regime (Williams and Smith, 1989) and was not an available option in the
23 previous VAMPER model version. To compensate for this, Kitover et al. (2013) had artificially introduced
24 the effect of snow cover via a surface offset of + 2°C. Not only was this an assumption based on a
25 number of previous reports and observations, but it had to be applied as an annual offset since the time
26 step was one year. This then demonstrates the need for the other enhancement, which is a sub-annual
27 timestep, where the seasonal changes in the ground thermal conditions can be captured, allowing for
28 representation of both the snow cover effect and the active layer. It should be noted that additional
29 coupling mechanisms are possible between *i*LOVECLIM components and VAMPER, which include
30 hydrology and the carbon cycle, but are not yet implemented at this time.

31 In addition to these VAMPER model enhancements, two global maps were produced (geo-processed
32 from the original maps to fit the horizontal grid of ECBilt) to be used as additional input parameters in
33 the *i*LOVECLIM model: geothermal heat flux and lithology.

34 Integrating permafrost into earth system models has become of increased interest since research has
35 acknowledged both its sensitivity to climate change along with carbon feedback implications. In fact,
36 Koven et al. (2013) recently reported on the Coupled Model Intercomparison Project phase 5, which
37 specifically looked at how different models represent the subsurface thermal dynamics and how well
38 this class of models simulate permafrost and active layer depth. Despite the fact that this study
39 introduced the variety of how different global coupled models capture permafrost, the overall

1 conclusion was that there is no clear ranking among their reviewed 15+ model configurations. This
2 shows that representing permafrost in earth system models still has some challenges, which Koven et al.
3 (2013) attribute primarily to modeling of both the atmosphere/ground energy exchange and the
4 subsurface thermal regime. Until recently, most simulations of permafrost were calibrated for regional
5 or local study such as Li and Koike (2003) on the Tibetan Plateau, Zhang et al. (2006) in Canada, and
6 Nicolsky et al. (2009) in Alaska. A growing number of studies are now modeling permafrost across a
7 global scale, namely these are from Lawrence and Slater (2005), Schaefer et al. (2011), and Dankers et al.
8 (2011). However, it should be noted that there is a difference between coupled models which actively
9 integrate the role of permafrost (including the thermal and/or carbon feedbacks) and models which
10 simply look at permafrost in a post-processing perspective, meaning they are forced by the predicted
11 temperature changes. It is the full coupling with integrated feedbacks which is of current interest but is
12 still in the early stages since, as just mentioned, there remain challenges to accurately represent
13 permafrost extent and active layer depths. The class of earth system models do not. Hence, it is the
14 authors' ultimate goal to fully couple ECBilt and VAMPERS within iLOVECLIM, where the results of the
15 present work serve as an important validation stage.

16 In the sections following, the two enhancements to the VAMPER model are explained. This includes
17 specific validation of the timestep change by comparing simulated annual active layer depths with
18 empirical-based estimates. The ECBilt-VAMPERS semi-coupling within the iLOVECLIM model is then
19 validated using a modern-day map of permafrost extent in the northern hemisphere and observed
20 permafrost thickness and subsurface temperatures values in boreholes.

21

22 **2 METHODS**

23 **2.1 VAMPER model**

24 **2.1.1. General Description**

25 VAMPER is a 1-d permafrost model developed to estimate permafrost thickness and was designed for
26 eventual full coupling with iLOVECLIM. Because it must fit a relatively coarse earth system model, it is
27 not suitable to undergo cumbersome parameterization schemes. It is meant rather as a generalized
28 model to simulate conceptual permafrost thickness based on the factors which most strongly dictate the
29 subsurface thermal regime. Most notable for our purposes and discussed by Farouki (1981), these
30 factors are mineral composition, water content, and temperature.

31 Other than what is specified below, construction of the VAMPER model has not changed and the
32 methods as described in Kitover et al., (2013) still apply. In particular, these include assuming only
33 conductive heat transfer in the subsurface, using an apparent heat capacity method for the latent heat
34 component, and employing well-established methods for finding the temperature-dependent thermal
35 properties of heat capacity and thermal conductivity (Farouki, 1981; Zhang et al., 2008). The subsurface
36 is assumed to be saturated (i.e. porosity equals the water content) and there is currently no
37 groundwater flow either horizontally or vertically between the soil layers.

1

2 2.1.2 VAMPER Model Enhancements

3 As compared to most permafrost modeling studies, there are few which have reproduced changes in
4 permafrost thickness over geologic time periods. In these cases, they assume a larger timestep in their
5 numerical simulations (usually one month or one year) (e.g., Osterkamp and Gosink, 1991; Lebreton et al.,
6 1994; Lunardini, 1995; Delisle, 1998) since they only need to force the models with the low frequency
7 changes in air temperature or ground temperature that occur over millennia, ~~in turn ignoring diurnal air~~
8 ~~temperature behavior~~. Since we are also interested in this timescale, we originally employed the same
9 reasoning: relying on large-signal paleoclimatic changes (Kitover et al., 2013). However, in ~~light~~ of
10 the coupling mechanism between ECBilt and the VAMPER model, it has become clear that the VAMPER
11 model should run on a 4-hr timestep. Doing this allows the VAMPER model to more closely follow the
12 response timescale of the atmosphere, the subsystem to which the VAMPER model is coupled, while
13 also allowing the numerical solution to converge since the thermal properties are temperature-
14 dependent and hence change on every timestep. Fortunately, being that the VAMPER model is
15 somewhat simplified, and hence flexible, this was done with some modifications to the original version.
16 Although the original makeup of the model was validated, it has since been necessary to perform an
17 additional verification (due to change in the timestep) while also enhancing the model with a snow layer
18 component. *Note that the VAMPER model with the snow enhancement is referred to as the VAMPERS*
19 *model. When referring to both/either versions, the “VAMPER(S)” term is used.*

20 **Timestep**

21 To illustrate the difference between applying the same annual average temperature forcing but with
22 two different timesteps (4-hr vs. yearly), a sensitivity test was performed (**Fig. 1a**). To generate the sub-
23 daily surface temperature forcing (4 hours), a year-long temperature time-series was calculated using a
24 standard sine function with constant amplitude 20°C and average annual temperature of -6 °C
25 (hereafter referred to as sensitivity run 1 or “sr1”), resulting in an annual range of temperatures
26 between -26 °C and 14°C. Therefore, the case with a yearly timestep, called “sr2”, simply used -6 °C
27 as the constant forcing. Besides the change in timestep and corresponding surface temperature forcing,
28 the thermal conductivity and heat capacity values were also ~~allowed~~ ~~subject~~ to differ since these
29 variables are temperature-dependent (**Fig. 1b**). However, heat flux and porosity parameter settings
30 were the same in both model runs. Each experiment was run until approximate equilibrium was reached
31 under the same constant (respective) forcing. We consider equilibrium to be when the geothermal heat
32 flux is approximately equal to the ground heat flux (what goes in = what goes out). Comparing the final
33 depth-temperature profiles between sr1 and sr2 shows a shift in the equilibrium depth-temperature
34 profile where using an annual timestep underestimates permafrost thickness by approximately 50
35 meters (**Fig. 1a**). This difference is attributed to occurrence of the thermal offset within the active layer
36 in sr1 (**Fig. 1b**), whereas sr2 cannot exhibit such seasonal phenomena. Since VAMPER is a simple model
37 (absence of vegetation, organics, an unsaturated subsurface, or temporally varying water content) we
38 can easily attribute the thermal offset to seasonal differences in thermal conductivity, whereas the
39 thermal conductivity of ice is four times that of unfrozen water and therefore the freezing front is

propagated more effectively than the warming front. This difference causes the mean annual subsurface temperature within the active layer to be gradually colder with depth. The offset is visible in the mean annual depth-temperature profile within the top meter of Figure 1b. Freezing and thawing within the active layer region causes seasonal variations in thermal conductivity, which is known as the thermal offset (Smith and Riseborough, 2002) and has been well-observed in permafrost environments (Romanovsky and Osterkamp, 1995; Brouchkov et al., 2005). This phenomenon is highly variable and depends on the subsurface material, water content, and climate such as the annual amplitude of the surface temperature forcing (French, 2007). The thermal offset is often expressed in a ratio format, also known as an n factor, where French (2007) reports that for bedrock this ratio is close to 1, for mineral soils between 0.6 and 0.9, and for organic soils anywhere between 0.3 and 1.

Active Layer

Since a sub-daily time step is used, the VAMPER model as expected produces an active layer. Most dynamical permafrost models that simulate near-surface behavior configure the parameter settings to specifically match locally observed data. Common parameterizations include organic and mineral layer thicknesses, which give soil properties such as porosity and bulk density, and unfrozen water content characteristics. Examples of these site-specific studies are numerous (e.g., Romanovsky and Osterkamp, 2000; Buteau et al., 2004; Ling and Zhang, 2004; Zhang et al., 2008; Nicolsky et al., 2009). Since VAMPER is not parameterized to capture site-specific behavior, it is challenging to assess the ability of the model to simulate active layer dynamics. Fortunately, there is a common calculation called the Stefan equation, used originally in engineering applications (Fox et al., 1992), to estimate the thickness of the active layer when the amount of energy input and thermal characteristics are known. From French (2007), the Stefan equation is defined as

$$AL = \sqrt{2\sigma k_{mw}/Q_i} \quad (1)$$

where AL (m) is the thickness of the active layer, σ is the cumulative thawing index (average ground surface temperature (°C) during the thaw season times the duration of thaw season (s)), and k_{mw} is the thermal conductivity of unfrozen soil (W (m K)⁻¹). Q_i (J m⁻³) is defined further as

$$Q_i = L\rho_m(W - W_u) \quad (2)$$

where L is the latent heat of fusion, ρ_m is the dry density of the soil (kg m⁻³), W is the total moisture content, and W_u is the unfrozen water content. **Table 1 below** gives the constant variable values applied in the Stefan Equation, which are the same values used in a comparable run for the VAMPER model-

Under different forcings as a function of both average annual ground surface temperature and annual amplitude, the VAMPER model's active layer thickness versus results using the Stefan Equation are shown in **Table 2**. It is clear when comparing the empirically-based results with the series of simulations, that the VAMPER model does a suitable job of reproducing annual active layer thickness.

Snowpack parameterization

1 | An additional [enhancement option](#) to the VAMPER model is the ability to extend the heat conduction
 2 | model into the snowpack when present. Prior to this, the surface offset, as illustrated in Smith and
 3 | Riseborough (2002), could not be applied in the VAMPER model. [Goodrich \(1982\) is a well-known study](#)
 4 | ~~which recognized the importance of including snow in numerical modeling of subsurface temperatures.~~

5 | The VAMPERS model uses snow water equivalent (swe) values (m) with corresponding density to
 6 | compute snow thickness layers. Snow water equivalent is the depth of water that would result from the
 7 | complete melting of snow. The precipitation simulated in ECBilt is computed from the precipitable water
 8 | of the first atmospheric layer (Goosse et al., 2010). When the air temperature is below 0 °C, the
 9 | precipitation is assumed to be snow. However, this ‘snow’ is only assumed to be frozen water, meaning
 10 | it lacks any quantifiable properties besides the actual precipitation amount, and as such is directly
 11 | considered the swe value. As a result, there ~~are~~ is an additional set of necessary functions when
 12 | coupled with VAMPERS to transfer ECBilt swe values into a snowpack thickness (Z) at time t :

$$13 \quad Z^t = \rho_w swe^t / \rho_s^t \quad (3)$$

14 | where ρ_w is water density and ρ_s snow density ([Lynch-Stieglitz, 1994](#)). The total snow density is
 15 | determined as a combination of old snow (expressed as swe^{t-1} from the previous timestep) and freshly
 16 | fallen snow at current timestep (expressed as swe^{fr}):

$$17 \quad \rho_s^t = (swe^{t-1} \rho_s^{t-1} + swe^{fr} \rho_{fr}) / swe^t \quad (4)$$

$$18 \quad swe^t = swe^{t-1} + swe^{fr} \quad (5)$$

19 | where ρ_{fr} is the density of fresh snow (150 kg m⁻³).

20 | There is snowpack metamorphism that occurs from a number of different processes. Notably, Dingman
 21 | (2002) distinguishes these as gravitational settling, destructive, constructive, and melt. However, as
 22 | these different changes occur at highly varying rates and under localized conditions (aspect, slope,
 23 | vegetation cover), it is nearly impossible to incorporate such processes in an [Earth System Model of](#)
 24 | [Intermediate Complexity \(-EMIC\)](#) such as *i*LOVECLIM. On the other hand, a snowpack always undergoes
 25 | densification over time and this effect should somehow be applied to the modeled snowpack.

26 | Therefore, we apply to the total snow density an empirical densification function due to mechanical
 27 | compaction. The maximum allowable density is 500 kg m⁻³, which ~~is considered a ‘ripe’ snowpack and~~
 28 | typically cannot hold any more liquid water (Dingman, 2002). The compaction equation used (e.g.
 29 | Pitman et al., 1991; Lynch-Stieglitz, 1994;) is as follows:

$$30 \quad \rho_s^t = \rho_s^{t-1} + \left(0.5 \times 10^7 \rho_s^{t-1} g N \exp \left[14.643 - \frac{4000}{\min(T+273.16, 273.16)} - 0.02 \rho_s^{t-1} \right] \right) \Delta t \quad (6)$$

31 | where g is gravity (9.82 m s⁻²), N (kg) is the mass of half the snowpack, T (°C) is the temperature of the
 32 | snowpack (the average temperature of the snow layer temperatures from the previous timestep), and
 33 | Δt is the timestep (s).

1 Three snow layers are then discretized from the total snow thickness, depending on whether it is above
 2 or below 0.2 m, as outlined in Lynch-Stieglitz (1994). Thermal properties are then calculated for each
 3 snow layer based on empirical formulas :

$$4 \quad K_s = 2.9 \rho_s^2 \quad (\text{Goodrich, 1982}) \quad (7)$$

$$5 \quad C_s = 1.9 \times 10^6 \rho_s / \rho_f \quad (\text{Verseghy, 1991}) \quad (8)$$

6 where K_s is the snow thermal conductivity and C_s is the snow heat capacity, and ρ_f is the density of ice
 7 (920 kg m⁻³). All three snow layer are subject to the same processes and simply depend on temperature,
 8 time, and thickness for their respective deformation and/or melting.

9 The following is a stepped description of the snow algorithm for the ECBilt-VAMPERS semi-coupling:

- 10 1. Calculate new snow density, Eq. (4) and Eq. (5), using any freshly fallen snow and old snow.
- 11 2. Apply compaction function, Eq. (6), to already existing snowpack
- 12 3. Calculate total snow thickness using Eq. (3).
- 13 4. Discretize the individual layer thicknesses based on total snow thickness.
- 14 5. Calculate thermal properties for each layer (Eq. (7) and Eq. (8)).
- 15 6. Use snow thicknesses and corresponding thermal properties as additional layers in the
- 16 VAMPERS model.

18 2.2 iLOVECLIM v 1.0

19 2.2.1 General Description

20 iLOVECLIM is a “code-fork” of LOVECLIM 1.2 (Goosse et al., 2010), both which belong to a class of
 21 climate models called EMICs (Claussen et al., 2002). This type of model, as summarized by Weber
 22 (2010), “describes the dynamics of the atmosphere and/or ocean in less detail than conventional
 23 General Circulation Models”. This simplification reduces computation time, thus making EMICs suitable
 24 for simulations on millennial timescales, incorporating the components with slow feedback effects, such
 25 as icesheets, vegetation, and permafrost. Different versions of LOVECLIM have successfully simulated
 26 past climates including the LGM (Roche et al., 2007), the Holocene (Renssen et al., 2005, 2009), and the
 27 last millennium (Goosse et al., 2005). Although there exist some different developments between
 28 iLOVECLIM and the LOVECLIM versions, both consist of the following coupled earth system
 29 components: the atmosphere (ECBilt), the ocean (CLIO), and vegetation (VECODE) (Fig. 2). Each
 30 component was originally developed separately and the reader is referred to Goosse et al., 2010 for a
 31 detailed description. Furthermore, iLOVECLIM more recently includes other optional components
 32 including an ice-sheet model (Roche et al., 2014) and a stable water isotopes scheme (Roche, 2013).

33 2.2.2 ECBilt-VAMPER(S) Coupling Description

34 The atmospheric component, ECBilt (Opsteegh et al., 1998), which the VAMPER(S) model is specifically
 35 coupled to, runs on a spectral grid with a triangular truncation (T21). This translates to a horizontal grid
 36 with a resolution of approximately 5.6 ° lat x 5.6 ° lon. The ECBilt-VAMPER(S) semi-coupling is done via

1 the air surface temperature from ECBilt at each timestep (4 hours), which the VAMPER(S) model uses as
 2 the ground temperature forcing. The air surface temperature is calculated within ECBilt as a function of
 3 the heat balance equation where the major heat fluxes across the air/surface interface are
 4 incorporated: sensible heat flux, latent heat flux, shortwave radiation, and longwave radiation. The air
 5 surface se-temperature iss-are only communicated to the VAMPER(S) model when the respective grid
 6 cell is classified as land with no overlying icesheet (i.e. Greenland/Antarctica at present day). Since the
 7 ECBilt air surface temperature is taken to be the VAMPER(S) model ground surface temperature is taken
 8 to be the ECBilt air surface temperature, there is no surface offset effect except when there is a
 9 snowpack. In this case, the air surface temperature from ECBilt is assumed to be above the snowthe
 10 snow surface temperature is taken to be the air surface temperature. This means the VAMPERS model
 11 ground temperature forcing is buffered via the three snowpack layers as discussed in Sect. 2.1.2. Using
 12 the ground surface temperature forcing, the VAMPER(S) model then calculates-computes the subsurface
 13 temperature profile. This calculation, via the implicitly solved heat equation with phase change
 14 capability, is fully described in Kitover et al. (2013). As VAMPER is a 1-D model, there is no lateral energy
 15 (heat/water) transfer between adjacent grid cells in the subsurface. Permafrost thickness is determined
 16 at an annual timestep using a computed average annual temperature profile, where any depth below or
 17 equal to 0°C is considered permafrost. Although there is a freezing point depression which may occur as
 18 a result of the local pressure or dissolved salts, we are consistent with the common thermal definition of
 19 permafrost from the International Permafrost Association: “ground (soil or rock and included ice or
 20 organic material) that remains at or below 0°C for at least two consecutive years”.

21 The land surface of ECBilt consists of a single “layer” which represents a volumetric storage capacity to
 22 generate surface runoff when full. This system is often referred to as a bucket model in previous text. As
 23 of currently, this bucket model, which is the surface hydrology in iLOVECLIM, is not coupled to
 24 VAMPERS. It would be a sensible next step to connect the active layer with this bucket model

25 The results presented in this current work is only a function of performing semi-coupled experiments
 26 and are means as an intermediary step to a fully coupled model in order to validate both VAMPERS and
 27 its ability to model permafrost extent and thickness. In future experiments, VAMPERS will be fully
 28 coupled to ECBilt. In this case then, aAt the end of each timestep, after VAMPER(S) would calculates-the
 29 new subsurface temperatures, the the ground heat flux is calculated and and return this value ed to
 30 ECBilt (Fig. 3) as one of the variable terms in the surface heat balance equation (among the other fluxes
 31 such as sensible heat flux, latent heat flux, etc.) at the air/ground interface, which in turn would beis
 32 used to obtain the air surface temperature for the next time step.-(Fig-3). The equations for this full
 33 coupling will be described in a future publication.

34 2.2.3 Geothermal Heat Flux

35 The VAMPER(S) model requires a geothermal heat flux as the lower surface boundary. In Kitover et al.
 36 (2013), a sensitivity analysis was performed to look at the equilibrium permafrost thickness as a result of
 37 varying the geothermal heat flux and found that thickness can increase by about 70 m with every
 38 decrease in flux of 10 mW m⁻². To obtain the geothermal heat flux for every cell in the ECBilt grid, we

1 used the recent publication of Davies (2013) who determined the median of heat flux estimates per
2 approximately $2^{\circ} \times 2^{\circ}$ latitude-longitude grid based on a combination of actual measurements,
3 modeling, and correlation assumptions. However, due to the mismatch of grid resolutions between
4 Davies (2013) and ECBilt, we determined for each ECBilt grid cell, a simple area-weighted average of the
5 Davies (2013) estimates. In other words, each of the Davies grid cells was assigned a weighing factor
6 based on the percentage of overlap with the ECBilt cells. Below is the original map from Davies (2013)
7 and the averaged map applied in the iLOVECLIM experiments (**Fig. 4**). A preliminary sensitivity analysis
8 between applying the geothermal heat flux map and applying the continental global average (approx. 60
9 mW m⁻²) showed no noticeable difference in permafrost distribution. This result is different, however,
10 than the noticeable sensitivity of geothermal heat flux on permafrost depth.

11 2.2.4 Porosity

12 Another variable needed to run the VAMPER(S) model is the porosity values throughout depth, which in
13 these experiments is down to 3000 meters deep. In previous VAMPER studies (Kitover et al., 2013;
14 Kitover et al., 2012), it was always assumed that the land subsurface was sedimentary rock, with a
15 porosity of 0.3, 0.4, or 0.5. However, as shown in Kitover et al. (2013), the porosity, or water content,
16 has a noticeable effect on equilibrium permafrost thickness. That sensitivity test showed about a 50 m
17 difference in permafrost thickness when the porosity values (assuming a saturated subsurface) ranged
18 between 0.3 and 0.5. Therefore, to both narrow our assumptions regarding the subsurface but still
19 maintain the simplification necessary for the coarse horizontal grid, an additional lithological
20 classification scheme was created as an additional VAMPER(S) model parameter. Using the recently
21 published Global Lithological Map Database (GLiM) from Hartmann and Moosdorf (2012), their original
22 seven categories were reclassified into 'Bedrock (Bed)', (e.g., granitic and metamorphic rock), and
23 'Sedimentary (Sed)' (e.g., sandstone, limestone) (**Table 3, Fig. 5**). In the case of 'Bed', the subsurface
24 would presumably be quite consolidated/compressed, resulting in a low water content (Almén et al.,
25 1986; Gleeson et al., 2014). 'Bed' was thus assigned a low porosity of 0.1, which based on sources that
26 showed depth profiles of bedrock sites (Schild et al., 2001; Nováková et al., 2012), stayed constant with
27 depth. On the other hand, similar to the case studies from Kitover et al. (2013), a depth porosity
28 function from Athy (1930) was applied for the 'Sed' class, where the surface porosity (Φ) was assumed
29 to be 0.40 and a decay constant (4×10^{-4}) in the exponential equation, representing the average for
30 sandy textured soil. Similar to application of the geothermal heat flux map, a preliminary sensitivity
31 analysis between applying the lithology map and applying a constant value (0.4) throughout the globe
32 showed only marginal differences in permafrost distribution. This result is different, however, than the
33 higher sensitivity of porosity on permafrost depth.

35 3 Validation of preindustrial permafrost thickness distribution

36 3.1 Experimental Setup

37 The model experiments are performed over the whole globe semi-coupled, which means that ECBilt
38 passes the air surface temperature values to the VAMPER(S) model (right side of **Fig. 3**) but no data is

1 returned to ECBilt (left side of **Fig. 3**), leaving the climate unaffected from permafrost or changes in
2 permafrost. This configuration, therefore, allows only the examination of the *i*LOVECLIM model to
3 reproduce current permafrost extent and depths as function of the currently established climate of the
4 *i*LOVECLIM model. Two different model runs were made: one without the snow enhancement or any
5 imposed surface offset (ECBilt-VAMPER coupling) and one with the snow enhancement (ECBilt-
6 VAMPERS coupling). These two are first compared in sect. 3.2.1 of the Results & Discussion below.

7 Because permafrost has a very slow thermal response (Lunardini, 1995) as compared to other
8 components in *i*LOVECLIM, VAMPER(S) is not run in a continuous (semi) coupling with ECBilt. Rather,
9 they are run together continuously for 100 years and then VAMPER(S) runs offline for 900 years using
10 the ECBilt average air surface temperature of the previous 100 years as the forcing. This asynchronous
11 cycle is repeated for thousands of years until approximate equilibrium between the ECBilt temperatures
12 and the VAMPER(S) model is reached. This scheme is illustrated in **Fig. 6** (adapted from a similar figure
13 in McGuffie and Henderson-Sellers (2005)). Equilibrium was determined ~~to be~~ when the lower boundary
14 heat flux approximately matches the annual average ground surface heat flux. This is also of course
15 when the permafrost thickness is stable. Although the model approaches a steady state through the
16 subsurface depth, we acknowledge that in reality, some of the permafrost regions are not at equilibrium
17 since they are responding to recent warming.

18 **3.2 Results and Discussion**

19 In order to verify the performance of the ECBilt-VAMPER(S) coupling within *i*LOVECLIM, a series of
20 equilibrium experiments were performed for the preindustrial (PI) climate (~ 1750 AD). For comparative
21 purposes, we assume the PI state of permafrost is similar enough to the current state of permafrost that
22 we used modern-day data to validate against the PI simulations. The simulated areal extent was
23 compared to present-day extent using the well-known “Circumarctic Map of Permafrost and Ground-Ice
24 Conditions” (Brown et al., 2014). Unlike the model validation done by Lawrence and Slater (2005), and
25 then subsequently critiqued by Burn and Nelson (2006), our simulations attempt to capture the extent
26 of both continuous and discontinuous permafrost. In addition, available borehole data, for sites within
27 the arctic/subarctic, were used to evaluate the simulated thicknesses. Therefore, there are essentially
28 two types of validation approaches: 1) horizontal (spatial extent) and 2) permafrost depth.

29 **3.2.1 Permafrost Distribution Validation**

30 The first validation demonstrates how well the *i*LOVECLIM model reproduces the modern-day
31 permafrost extent by overlaying the simulated results on the map from Brown et al. 2014.

32 Using a comparison between the different couplings (**Fig. 7**), it is clear that the experiment where the
33 ECBilt- VAMPER semi-coupling (no snow-~~enhancement~~option and no imposed surface offset) is used
34 overestimates permafrost extent while employing the ECBilt -VAMPERS version underestimates it. This
35 swing of inaccuracy is at least partially due the result of to simply attempting to match results from a
36 low resolution grid to spatial coverage of much higher resolution. In addition, we expect some
37 inaccuracy since we cannot parameterize the snowpack characteristics and more importantly, the
38 nature of the snowmelt. As opposed to our generalized approach described earlier, high resolution

1 snowmelt models are fitted to observational data by analyzing, for example, the physics of
 2 accumulation, areal distribution, and snow-soil interactions. Therefore, it is arguable from Fig. 7 and the
 3 recognized discrepancies in generalizing snow model details, whether the better option is to include ~~the~~
 4 snowpack in VAMPERS or not, ~~since neither 'swing' is very exact.~~ However, as long as the VAMPERS
 5 model is doing a reasonable job, we contend it is a better option an improvement over merely applying
 6 artificial offsets or assuming none at all since snow plays a critical role in the ground thermal conditions
 7 and should be represented. Further, with the snow option is enhancement, changing precipitation
 8 patterns that are often the byproduct of a shifting climate would otherwise have no effect on the
 9 subsurface thermal conditions. In other words, the role of snow cover is likely more noticeable in using
 10 the ECBilt-VAMPERS coupling when doing transient experiments. From this point forward, all analysis is
 11 done using results from the ECBilt-VAMPERS coupling (i.e. *with* the snow option enhancement).

12 Employing the snow enhancement option in the ECBilt-VAMPERS coupling produces the surface offset
 13 that would naturally occur from the snowpack (Goodrich, 1982; Smith and Riseborough, 2002). The
 14 simulated global distribution of this offset is shown in Fig. 8. It is determined by calculating the
 15 difference between the mean annual ground temperature (MAGT) using the ECBilt-VAMPERS coupling
 16 and the MAGT using the ECBilt-VAMPER coupling (no snow enhancement option and no imposed
 17 offset). Although the maximum mean annual surface offset is about 12 °C, the average among all the
 18 grid cells that had snow cover is about 2.7 C, which is close to our original applied offset of 2 °C in
 19 Kitover et al., (2013). Values between 1 °C and 6 °C were reported early on by Gold and Lachenbruch
 20 (1973). Monitoring studies of the air-ground temperature relationship also fall within this range e.g.,
 21 Beltrami and Kellman (2003), Bartlett et al., (2005), Grundstein et al., (2005), Zhang (2005). However,
 22 larger values of 10 °C have been recorded in Alaska (Lawrence and Slater, 2010).

23 In addition to the offset imposed by incorporation of a snowpack, there are a number of factors which
 24 have been commonly recognized in affecting the surface offset and hence should be part of the air-
 25 ground coupling. Depending on the scale of interest, the magnitude of these can vary but a standard list
 26 includes surface organic layer, vegetation, overlying water bodies, and wind. It should be recognized
 27 that within ECBilt, some of these factors are reflected in the air surface temperature (notably wind and a
 28 simplified vegetation scheme) but the others are absent. In addition, coupling the ECBilt surface
 29 hydrology to the groundwater storage would affect both the ground thermal regime and hydrological
 30 regime. In the first case, subsurface water content affects the thermal properties of the soil. In
 31 particular, the conductivity of organics have high variation seasonally. In the second instance, frozen
 32 ground is impermeable, allowing little or no subsurface water storage, in turn affecting runoff flowrates
 33 and timing.

34 The permafrost distribution simulated by jLOVECLIM can be matched against results from a study
 35 comparing a suite of earth system models, namely the Coupled Model Intercomparison Project phase 5
 36 (CMIP5) (Koven et al., 2013). This report gives the simulated preindustrial permafrost areas under a
 37 number of different earth system climate models and configurations. Compared to the results from
 38 jLOVECLIM, some of the other models' simulated permafrost distributions cover more area while some
 39 cover less. The maximum is reported as $28.6 \times 10^6 \text{ km}^2$ and minimum $2.7 \times 10^6 \text{ km}^2$. The simulation by
 40 jLOVECLIM yields approximately $20.3 \times 10^6 \text{ km}^2$. This is a reasonably comparable estimate considering
 41 almost 80 % (14/18) of the model area extents from Koven et al. (2012) fall within 40% ($12 - 28 \times 10^6$

Formatted: No Spacing, Justified

Formatted: Font: Italic

Formatted: Font: Italic

Formatted: Font: Italic

1 km²) of our model estimates. According to discussion by Koven et al., (2012), most of the variation seen
2 among the compared earth system models is primarily attributed to the subsurface modeling
3 techniques, such as water content, using a latent heat term, and differing soil thermal conductivities.
4 Secondary causes are attributed to the air-ground coupling such as incorporation of organics and a
5 snowpack (bulk or multilayer). These conclusions are not different from our own study in that 1)
6 snowpack plays a marked role in permafrost modeling and inclusion/exclusion will impact the results, 2)
7 the air-ground coupling is also a source of potential mismatch (discussed further in section 3.2.2).
8
9

10 3.2.2 Permafrost Thickness Validation

11 The second validation examines the simulated depth of permafrost using borehole data taken from the
12 Global Terrestrial Network for Permafrost (GTN-P; www.gtnp.org). The scatterplot (Fig. 9) shows all the
13 observed borehole measurements mapped in Fig. 10 versus the corresponding permafrost depth
14 simulated by iLOVECLIM. It is clear that there is a larger divergence between modeled and observed
15 depths for the deeper permafrost than for the more shallow observations, where some points are
16 relatively overestimated (> 300 m) and some very underestimated (>700 m). There are a number of
17 reasons to explain the mismatch, which can occur in the borehole data and/or the model data. The first
18 explanation is that the borehole estimates have a given range of uncertainty since measurement
19 techniques and subsequent interpretations are subject to error. Osterkamp and Payne (1981) describe
20 in detail potential errors associated with the freezing point depression, thermal disturbance, and
21 lithology.

22 The second cause is that we assumed implicitly that the observed permafrost depths are at equilibrium
23 with the current (or PI; preindustrial) climate state. This is probably why there is a striking mismatch at
24 the central Siberian site (66° 26' 2" N, 112° 26' 5" E) (point 1, Fig. 9), where the permafrost is estimated
25 from the borehole data to be 1000 m thick while the corresponding modeled value is only about 375 m.
26 It is very likely that, like much of the Siberian permafrost, this permafrost developed from the preceding
27 glacial period (Kondratjeva et al., 1993). Another example concerns western Siberia, (points 2 through 4,
28 Fig. 9), which is an area well documented for having relict permafrost (Zemtsov and Shamakhov, 1992;
29 Ananjeva et al., 2003). It is also identified in the "Circumarctic Map of Permafrost and Ground-Ice
30 Conditions" (Brown et al., 2014) and "The Last Permafrost Maximum (LPM) map of the Northern
31 Hemisphere" (Vandenbergh et al., 2014). But it should be noted that not all the relict permafrost in
32 western Siberia is of late Pleistocene origin and may be from earlier cold stages (Zemtsov and
33 Shamakhov, 1992; French, 2007).

34 Another reason for some discrepancies between modeled and observed data is that high-resolution
35 features in the landscape and topography cannot be captured by iLOVECLIM due to the limited spatial
36 resolution and hence, a small set of model parameters. Such factors as vegetation and organic layer,
37 which can vary due to local topography and micro-climatic conditions, have been shown to affect the
38 active layer and ground thermal regime (Shur and Yorgenson, 2007; Fukui et al., 2008; Lewkowicz et al.,
39 2011; Wang et al., 2014). Consequently, given a specific borehole site, some discrepancy in the
40 permafrost thickness estimate will likely occur between our simplified interpretation and that which
41 results from including more complex and local interactions. It is possible, for example, that the observed

1 value for point 5 (720 m) is a function of higher elevation since it is from a borehole site in the Russia
2 Highlands but this relatively local elevation effect may not be a strong enough signal in the *i*LOVECLIM
3 surface temperatures, and hence is underestimated.

4 The other outlying points (points 6 and 7, **Fig. 9**) occur in Canada but as opposed to the relict sites as
5 mentioned above, *i*LOVECLIM overestimates the permafrost thickness quite noticeably. These
6 discrepancies, both occurring at high latitudes of 80 °N and 76 °N , reveal that VAMPERS is probably not
7 reproducing the subsurface temperatures well for this area. For example, a report for the specific
8 borehole (Gemini E-10; point 6, **Fig. 9**) calculated the geothermal gradient to be approximately 0.04
9 °C/m (Kutasov and Eppelbaum, 2009) whereas our model result for the corresponding grid space found
10 a gradient of approximately 0.03 °C/m. Although this difference may seem small, it hints at either a
11 necessary increase in the averaged geothermal heat flux used in the model or a change in the
12 subsurface thermal properties (increase in thermal conductivity), which could be altered by an
13 adjustment in the VAMPERS water content.

14

15 **3.2.3 Climate analysis**

16 Finally, the remaining possibility to explain inaccuracies between the modeled results and the observed
17 results (both in reproducing spatial extent and permafrost thickness) is the *i*LOVECLIM climate. Results
18 of the VAMPER model, above all other parameter settings, are most dependent on the mean annual
19 ground surface temperature, as shown in the sensitivity study from Kitover et al. (2013), so if there
20 exists biases or discrepancies within the forcing, it will be reflected in the semi-coupled output. For this
21 portion of our analysis, we took observed mean annual ground temperature (MAGT) measurements
22 from again the GTN-P (IPY Thermal State of Permafrost Snapshot, IPA 2010) . As a result, we composed a
23 1:1 comparison between the observed MAGT and the corresponding simulated MAGT at the same
24 approximate depth and location (**Fig. 11**). **Figure 12** shows a map of the selected GTN-P measurements.
25 All the temperature comparisons are within the top thirty meters of the subsurface and therefore reflect
26 the present or very recent climate as opposed to the deeper temperatures (i.e., > 150 m) that,
27 depending on subsurface thermal diffusivity and surface temperature perturbations, can reflect
28 historical temperatures of at least one hundred years ago (Huang et al., 2000) and up to tens of
29 thousands of years (Ter Voorde et al., 2014).

30 Overall, **Fig. 11** illustrates that ECbilt-VAMPERS does a reasonable job of predicting shallow subsurface
31 temperatures since a majority of the points fall near the 1:1 line. This result, therefore, supports the
32 notion that the preindustrial climate is well represented by *i*LOVECLIM. The points of Kazakhstan and
33 Mongolia, and a few others in Russia, have a warm bias in the forcing (simulated is warmer than
34 observed), which is probably due to an inaccurate representation of elevation temperature changes in
35 *i*LOVECLIM, since many of those sites are at elevations above 1000 m. Even applying the lapse rate for a
36 standard profile (6.5 C / km; McGuffie & Henderson-Sellers, 2013) would presumably make a significant
37 difference on the depth since earlier sensitivity tests (Kitover et al., 2013) showed an average 55 m
38 increase in equilibrium permafrost depth for every 1 °C colder. On the other hand, many of the other
39 points show that predicted subsurface temperatures are on average a few degrees colder than the
40 observed, leading to the most obvious conclusion that a cold bias exists in the *i*LOVECLIM climate.

Formatted: Space After: 0 pt

1 ~~Although it should be noted that the cold bias, most obvious for Canada and Alaska, is congruent to the~~
2 ~~overestimation in permafrost thickness evident from the geographic breakdown illustrated in Fig. 10, it,~~
3 ~~However, this~~ has not previously been substantiated in former analyses of LOVECLIM or iLOVECLIM so it
4 is more likely that such a discrepancy is due to the air-ground coupling as opposed to simply the air
5 surface temperature forcing. Indeed, there a number of other (sub)surface processes not included in
6 the current ECBilt-VAMPERS coupling which may reduce the apparent cold bias. These effects primarily
7 alter the seasonal behavior of the thermal diffusivity in the subsurface and have been well-documented
8 in observational studies (Williams and Burn, 1996; Woo and Xia, 1996; Fukui et al., 2008). ~~These effects~~
9 ~~are also identified in~~ Smith and Riseborough (2002) ~~simplified these mechanisms into as both~~ the
10 surface offset (air to ground surface) and the thermal offset (ground surface to top of the permafrost).
11 Due to minimal parameterization of the VAMPERS model, these offsets may be somewhat overlooked.

12 ~~It should be noted that the cold bias, most obvious for Canada and Alaska, is congruent to the~~
13 ~~overestimation in permafrost thickness evident from the geographic breakdown illustrated in Fig. 10.~~
14 For now, the average range of error between observed and predicted is about 2.6 °C. Given that the
15 comparisons are between point-based observations and large grid cell values, meant to represent a
16 relatively large surface area, some variability is expected to occur.

18 4 Next Steps

19 The results of this paper demonstrate the ability of ECBilt-VAMPERS semi-coupling within iLOVECLIM to
20 model current permafrost distribution and thickness. The next step is to analyze the feedback that
21 permafrost changes have on the climate. This has been of particular interest of the last decade since it is
22 clear that specific feedbacks exists, most notably the release of locked-up carbon in the atmosphere as
23 permafrost degrades (Anisimov, 2007). The initial method behind a full coupling would be to integrate
24 the additional coupling mechanisms, shown in Fig. 3, and reanalyze the equilibrium results (since a full
25 coupling would likely lead to an altered equilibrium permafrost state). In addition, the feedback effects
26 would be most visible during millennial-scale transient climate shifts, when major permafrost
27 degradation and/or disappearance is likely to occur.

29 5 Conclusions

30 Enhancements have been made to the VAMPER model to make possible the first version of the ECBilt-
31 VAMPERS semi-coupling. The change in timestep to 4 hours was necessary to match the timestep of
32 ECBilt and allow the seasonal effects, notably snow cover and the active layer, to be reflected in the
33 simulation of permafrost. The predicted annual active layer from the stand-alone VAMPER model, under
34 different temperature forcings, compare well with results from the Stefan equation. We also described
35 the snow ~~enhancement option~~, which introduces the thermal insulation effects and changes in the
36 thermal properties of snow over time due to varying snow densities. In addition, we developed two new

1 maps: geothermal heat flux and porosity. Incorporating these parameters at a global scale was an
2 important step in improving the horizontal spatial variability of permafrost thickness/distribution while
3 also maintaining the simplicity and efficiency of ECBilt-VAMPERS.

4 Using a semi-coupled ECBilt-VAMPER(S) component within *i*LOVECLIM, equilibrium experiments for the
5 PI climate show that when the snow component is included in the VAMPER model, the permafrost
6 extent is noticeably reduced while the average offset of 2.7 °C is comparable to previous reports. We
7 then compared both permafrost thickness estimates and subsurface temperatures to corresponding
8 observed values. Considering that we are comparing point measurements to gridcell-based values, the
9 simulations are quite reasonable. There are some discussion points around the most obvious
10 discrepancies. One is that the relatively coarse horizontal ECBilt grid will never perfectly match the
11 sensitivity of permafrost occurrence and depth due to local factors. This is also the case in the air-land
12 temperature coupling, where some of the local effects will simply not be present in an EMIC. Similarly,
13 when *i*LOVECLIM does not accurately represent the environmental lapse rate in areas of higher
14 elevation, the occurrence of permafrost in these areas are overlooked by the VAMPERS model. Finally,
15 some of the observed permafrost depths are not a function of the present (PI) climate, but rather a
16 relict presence from previous cold periods. Therefore, when comparing measured to simulated results,
17 some underestimations expectedly occurred. It is only with millennial-scale transient *i*LOVECLIM model
18 runs that we can simulate, for example in areas of West Siberia, how permafrost evolved over periods of
19 major climate change.

20

21 **6 Code availability**

22 The *i*LOVECLIM (version 1.0) source code is based on the LOVECLIM model version 1.2 whose code is
23 accessible at <http://www.elic.ucl.ac.be/modx/elic/index.php?id=289>. The developments on the
24 *i*LOVECLIM and VAMPER(S) source code are hosted at <https://forge.ipsl.jussieu.fr/ludus> but are not
25 publicly available due copyright restrictions. Access can be granted on demand by request to D. M.
26 Roche (didier.roche@lsce.ipsl.fr).

1 **References**

2

3 Almén, K., Andersson, J., Carlsson, L., Hansson, K., and Larsson, N.: Hydraulic testing in crystalline rock.
 4 A comparative study of single-hole test methods, Swedish Nuclear Fuel and Management Company,
 5 Uppsala, Sweden, SKB Technical Report 86-27, 190 pp., 1986.

6 Ananjeva (Malkova), G.V., Melnikov, E.S., and Ponomareva, O.E.: Relict permafrost in the central part of
 7 western Siberia, in: Proceedings of 8th International Conference on Permafrost, Zurich, Switzerland, 5-8,
 8 2003.

9 Anisimov, O.A.: Potential feedback of thawing permafrost to the global climate system through methane
 10 emission, Environ. Res. Lett., 2, 045016, doi:10.1088/1748-9326/2/4/045016, 2007.

11 Athy, L.F.: Density, porosity, and compaction of sedimentary rocks, Am. Assoc. Petrol. Geol. Bull, 14, 1-
 12 24, 1930.

13 Bartlett, M.G., Chapman, D.S., and Harris, R.N.: Snow effect on North American ground temperature
 14 1950-2002, J. Geophys. Res., 110, F03008, doi: 10.1029/2005JF000293, 2005.

15 Beltrami, H. and Kellman, L.: An examination of short- and long-term air-ground temperature coupling,
 16 Global Planet. Change, 38, 291-303, 2003.

17 Burn, C.R and Nelson, F.E.: Comment on "A projection of severe near-surface permafrost degradation
 18 during the 21st century" by David M. Lawrence and Andrew G. Slater, Geophys. Res. Lett., 33, L21503,
 19 doi:10.1029/2006GL027077, 2006.

20 Buteau, S., Fortier, R., Delisle, G., and Allard, M.: Numerical simulation of the impacts of climate
 21 warming on a permafrost mound, Permafrost Periglac., 15, 41-57, 2004.

22 Brouchkov, A., Fukuda, M., Iwahana, G., Kobayashi, Y., and Konstantinov, P.: Thermal conductivity of
 23 soils in the active layer of eastern Siberia, Permafrost Periglac., 16, 217-222, 2005.

24 Brown, J., Ferrians, O., Heginbottom, J.A., and Melnikov, E.: Circum-Arctic Map of Permafrost and
 25 Ground-Ice Conditions, National Snow and Ice Data Center, Boulder, CO, 2014.

26 Claussen, M., Mysak, L.A., Weaver, A.J, Crucifix, M., Fichet, T., Loutre, M.-F., Weber, S.L., Alcamo, J.,
 27 Alexeev, V.A., Berger, A., Calov, R., Ganopolski, A., Goosse, H., Lohmann, G., Lunkeit, F., Mokhov, I.I.,
 28 Petoukhov, V., Stone, P., and Wang, Z.: Earth system models of intermediate complexity: closing the gap
 29 in the spectrum of climate system models, Clim. Dynam., 18, 579-186, 2002.

30 [Dankers, R., Burke, E.J. and Price J.: Simulation of permafrost and seasonal thaw depth in the JULES land
 31 surface scheme, The Cryosphere, 5, 773-790.](#)

32 Davies, J.H.: Global map of solid earth heat flow, Geochim. Geophys. Geosy., 14, 4608-4622, doi:
 33 10.1002/ggge.20271, 2013.

Formatted: English (United States)

- 1 Delisle, G.: Numerical simulation of permafrost growth and decay, *J. Quaternary Sci.*, 13, 325-333, 1998.
- 2 Dingman, S.L.: *Physical Hydrology*, Second Edition, Prentice Hall, Upper Saddle River, N.J., 2002.
- 3 Farouki, O.T.: Thermal properties of soils, Cold Regions Research and Engineering Laboratory, Hannover,
4 N.H., CRREL Report 81-1, 136 pp., 1981.
- 5 Fox, J.D.: Incorporating freeze-thaw calculations into a water balance model, *Water Resour. Res.*, 38,
6 2229-2244, 1992.
- 7 French, H.M.: *The Periglacial Environment*, Third Edition, Jon Wiley & Sons Ltd, West Sussex, England,
8 2007.
- 9 Fukui, K., Sone, T., Yamagata, K., Otsuki, Y., Sawada, Y., Vetrova, V., and Vyatkina, M.: Relationships
10 between permafrost distribution and surface organic layers near Esso, Central Kamchatka, Russian Far
11 East, *Permafrost Periglac.*, 19, 85-92, doi: 10.1002/ppp.606, 2008.
- 12 Gleeson, T., Moosdorf, N., Hartmann, J., and van Beek, L. P. H.: A glimpse beneath earth's surface:
13 Global HYdrogeology MaPS (GLHYMPS) of permeability and porosity, *Geophys. Res. Lett.*, 41,
14 2014GL059856, doi:10.1002/2014gl059856, 2014.
- 15 Gold, L.W. and Lachenbruch, A.H.: Thermal conditions in permafrost - a review of North American
16 literature, in: *Permafrost: The North American Contribution to the Second International Conference*,
17 Yakustsk, USSR, 13-28 July 1973, 3-23, 1973.
- 18 Goodrich, L.E.: The influence of snow cover on the ground thermal regime, *Can. Geotech. J.*, 19, 421-
19 432, 1982.
- 20 Gosse, H., Renssen, H., Timmermann, A., and Bradley, R. S.: Internal and forced climate variability
21 during the last millennium: a model-data comparison using ensemble simulations, *Quaternary Sci. Rev.*,
22 24, 1345–1360, 2005.
- 23 Gosse, H., Brovkin, V., Fichefet, T., Haarsma, R., Huybrechts, P., Jongma, J., Mouchet, A., Selten, F.,
24 Barriat, P.Y., Campin, J., Deleersnijder, E., Driesschaert, E., Goelzer, H., Janssens, I., Loutre, M., Morales
25 Maqueda, M.A., Opsteegh, T., Mathieu, P., Munhoven, G., Pettersson, E.J., Renssen, H., Roche, D.M.,
26 Schaeffer, M., Tartinville, B., Timmermann, A., and Weber, S.L.: Description of the earth system model of
27 intermediate complexity LOVECLIM version 1.2, *Geosci. Model Dev.*, 3, 603-633, DOI: 10.5194/gmd-3-
28 603-2010, 2010.
- 29 Grundstein, A., Todhunter, P., and Mote, T.: Snowpack control over the thermal offset of air and soil
30 temperatures in eastern North Dakota, *Geophys. Res. Lett.*, 32, L08503, doi:10.1029/2005GL022532,
31 2005.
- 32 Hartmann, J. and Moosdorf, N.: The new global lithological map database GLIM: A representation of
33 rock properties at the Earth surface, *Geochem. Geophys. Geosy.*, 13, Q12004,
34 doi:10.1029/2012GC004370, 2012.

- 1 Huang, S., Pollack, H.N., and Shen, P.: Temperature trends over the past five centuries reconstructed
2 from borehole temperatures, *Nature*, 403, 756-758, 2000.
- 3 Kitover, D.C., Renssen, H., Vandenberghe, J., and van Balen, R.T.: Modeling permafrost response of the
4 last glacial termination: first results of the VAMPER model, in: Proceedings of the 10th International
5 Conference on Permafrost, Salekhard, Russia, 25-29 June 2012, 209-214, 2012.
- 6 Kitover, D.C., van Balen, R.T., Roche, D.M., Vandenberghe, J., and Renssen, H.: New estimates of
7 permafrost evolution during the last 21 k years in Eurasia using numerical modelling, *Permafrost*
8 *Periglac.*, 24, 286-303, 2013.
- 9 Kondratjeva, K.A., Khrutsky, S.F., and Romanovsky, N.N.: Changes in the extent of permafrost during the
10 late Quaternary period in the territory of the former Soviet Union, *Permafrost Periglac.*, 4, 113-119,
11 1993.
- 12 [Koven, C.D., Riley, W.J., and Stern, A.: Analysis of permafrost thermal dynamics and response to climate
13 change in the CMIP5 earth system models, *Journal of Climate*, 26, 1877-1900, doi: 10.1175/JCLI-D-12-
14 00228.1, 2013.](#)
- 15 Kutasov, I.M. and Eppelbaum, L.V.: Estimation of geothermal gradients from single temperature log-field
16 cases, *J. Geophys. Eng.*, 6, 131-135, doi: 10.1088/1742-2132/6/2/004, 2009.
- 17 Lawrence, D.M. and Slater, A.G.: A projection of severe near-surface permafrost degradation during the
18 21st century, *Geophys. Res. Lett.*, 32, L24401, doi: 10.1029/2005GL025080, 2005.
- 19 Lawrence, D.M. and Slater, A.G.: The contribution of snow condition trends to future ground climate,
20 *Clim. Dyn.*, 34, 969-981, doi: 10.1007/s00382-009-0537-4, 2010.
- 21 Lebret, P., Dupas, A., Clet, M., Coutard, J., Lautridou, J., Courbouleix, S., Garcin, M., Levy, M., and Van
22 Vliet-Lanoë, B.: Modelling of permafrost thickness during the late glacial stage in France: preliminary
23 results, *Can. J. Earth Sci.*, 31, 959-968, 1994.
- 24 Lewkowicz, A.G., Etzelmüller, B., and Smith, S.: Characteristics of discontinuous permafrost based on
25 ground temperature measurements and electrical resistivity tomography, Southern Yukon, Canada,
26 *Permafrost Periglac.*, 22, 320-342, doi: 10.1002/ppp.703, 2011.
- 27 [Li, X. and Koike, T.: Frozen soil parameterization in SIB2 and its validation with GAME-Tibet observations,
28 *Cold Reg. Sci. Technol*, 36, 165-182, doi:10.1016/S0165-232X\(03\)00009-0, 2003.](#)
- 29 Ling, F. and Zhang, T.: A numerical model for surface energy balance and thermal regime of the active
30 layer and permafrost containing unfrozen water, *Cold Reg. Sci. Technol.*, 38, 1-15, 2004. Lunardini, V.J.
31 Permafrost formation time, Cold Regions Research and Engineering Laboratory, Hannover, N.H., CRREL
32 Report 95-8, 1995.
- 33 Lynch-Stieglitz, M.: The development and validation of a simple snow model for the GISS GCM, *J.*
34 *Climate*, 7, 1842-1855, 1994.

- 1 McGuffie, K. and Henderson-Sellers, A.: A Climate Modelling Primer, John Wiley & Sons, Ltd., West
2 Sussex, England, 2013.
- 3 Nicolsky, N.J., Romanovsky, V.E., and Panteleev, G.G.: Estimation of soil thermal properties using in-situ
4 temperature measurements in the active layer and permafrost, , Cold Reg. Sci. Technol, 55, 120-129,
5 2009.
- 6
- 7 Nováková, L., Sosna, K., Brož, M., Najser, J., and Novák, P.: The matrix porosity and related properties
8 of a leucocratic granite from the Krudum Massif, West Bohemia, Acta Geodyn. Geomater., 9, 521-540,
9 2012.
- 10 Opsteegh, J., Haarsma, R., Selten, F., and Kattenberg, A.: ECBILT: A dynamic alternative to mixed
11 boundary conditions in ocean models, Tellus, 50, 348–367, 1998.
- 12 Osterkamp, T.E. and Gosink, J.P.: Variations in permafrost thickness in response to changes in
13 paleoclimate, J. Geophys. Res., 96, 4423-4434, 1991.
- 14 Osterkamp, T.E. and Payne, M.W.: Estimates of permafrost thickness from well logs in northern Alaska,
15 Cold Reg. Sci. Technol, 5, 13-27, 1981.
- 16 Pitman, A.J., Yang, Z-L., Cogley, J.G., and Henderson-Sellers, A.: Description of bare essentials of surface
17 transfer for the Bureau of Meteorological Research Centre AGCM, BRMC, Australia, BMRC Research
18 Report 32, 117 pp., 1991.
- 19 Renssen, H., Goosse, H., Fichefet, T., Brovkin, V., Driesschaert, E., and Wolk, F.: Simulating the Holocene
20 climate evolution at northern high latitudes using a coupled atmosphere-sea ice-ocean-vegetation
21 model, Clim. Dynam., 24, 23–43, doi: 10.1007/s00382-004-0485-y, 2005.
- 22 Renssen, H., Seppä, H., Heiri, O., Roche, D. M., Goosse, H., and Fichefet, T.: The spatial and temporal
23 complexity of the Holocene thermal maximum, Nat. Geosci., 2, 411–414, doi: 10.1038/ngeo513, 2009.
- 24 Roche, D.M.: $\delta^{18}\text{O}$ water isotope in the iLOVECLIM model (version 1.0) – Part 1: Implementation and
25 verification, Geosci. Model Dev., 6, 1481-1491, doi:10.5194/gmd-6-1481-2013, 2013.
- 26 Roche, D.M., Dokken, T.M., Goosse, H., Renssen, H., and Weber, S.L.: Climate of the last glacial
27 maximum: sensitivity studies and model-data comparison with the LOVECLIM coupled model, Clim. Past,
28 3, 205-224, 2007.
- 29 Roche, D.M., Dumas, C., Bügelmayer, M., Charbit, S., and Ritz, C.: Adding a dynamical cryosphere to
30 iLOVECLIM (version 1.0): coupling with the GRISLI ice-sheet model, Geosci. Model Dev., 7, 1377-1394,
31 doi: 10.5194/gmd-7-1377-2014, 2014.
- 32 Roche, D.M., Renssen, H., Paillard, D., and Levvasseur, G.: Deciphering the spatio-temporal complexity
33 of climate change of the last deglaciation: a model analysis, Clim. Past, 7, 591-602, doi: 10.5194/cp-3-
34 205-2007, 2011.

- 1 Romanovsky, V.E. and Osterkamp, T.E.: Interannual variations of the thermal regime of the active layer
2 and near-surface permafrost in northern Alaska, *Permafrost Periglac.*, 6, 313-335, 1995.
- 3 [Schaefer, K., Zhang, T., Bruhwiler, L. and Barret, A.P.: Amount and timing of permafrost carbon release in
4 response to climate warming, *Tellus Series B Chemical and Physical Meteorology* , 63B, 165-180, 2011.](#)
- 5 Schild, M., Siegesmund, S., Vollbrecht, A., and Mazurek, M.: Characterization of granite matrix porosity
6 and pore-space geometry by in situ and laboratory methods, *Geophys. J. Int.*, 146, 111-125, 2001.
- 7 Shur, Y.L. and Jorgenson, M.T.: Patterns of permafrost formation and degradation in relation to climate
8 and ecosystems, *Permafrost Periglac.*, 18, 7-19, doi: 10.1002/ppp.582, 2007.
- 9 Smith, M.W. and Riseborough, D.W.: Climate and the limits of permafrost: A zonal analysis, *Permafrost
10 Periglac.*, 13, 1-15, 2002.
- 11 Ter Voorde, M., van Balen, R., Lujendijk, E., and Kooi, H.: Weichselian and Holocene climate history
12 reflected in temperatures in the upper crust of the Netherlands, *Neth. J. Geosci.*, 93, 107-117,
13 doi:10.1017/njg.2014.9, 2014.
- 14 Vandenberghe, J., French, H.M., Gorbunov, A., Marchenko, S., Velichko, A.A., Jin, H., Cui, Z., Zhang, T.,
15 and Wan, X.: The Last Permafrost Maximum (LPM) map of the Northern Hemisphere: permafrost extent
16 and mean annual temperatures, 25-17 ka BP, *Boreas*, 43, 652-666, doi: 10.1111/bor.12070, 2014.
- 17 Verseghy, D.L.: CLASS-A Canadian land surface scheme for GCMS I. Soil model, *Int. J. Climatol.*, 11, 111-
18 133, 1991.
- 19 Wang, G., Mao, T., Chang, J., and Du, J.: Impacts of surface soil organic content on the soil thermal
20 dynamics of alpine meadows in permafrost regions: data from field observations, *Geoderma*, 232-234,
21 414-425, doi: 10.1016/j.geoderma.2014.05.016, 2014.
- 22 Weber, S.L.: The utility of Earth system Models of Intermediate Complexity (EMICs), *WIREs Climate
23 Change*, 1, 243-252, doi: 10.1002/wcc.24, 2010.
- 24 Williams, D.J. and Burn, C.R.: Surficial characteristics associated with the occurrence of permafrost near
25 Mayo, Central Yukon Territory, Canada, *Permafrost Periglac.*, 7, 193-206, 1996.
- 26 Williams, P.J. and Smith, M.W.: *The Frozen Earth: Fundamentals of Geocryology*, Cambridge University
27 Press, Cambridge, England, 2007.
- 28 Woo, M.K. and Xia, Z.: Effects of hydrology on the thermal conditions of the active layer, *Nordic
29 Hydrology*, 27, 129-142, 1996.
- 30 Zemtsov, A.A. and Shamakhov, A.F.: Characteristics of relict permafrost on the west Siberian plain, *Polar
31 Geography and Geology*, 17, 245-250, 1993.
- 32 Zhang, T.: Influence of the seasonal snow cover on the ground thermal regime: an overview, *Rev.
33 Geophys.*, 43, RG4002, doi:10.1029/2004RG000157, 2005.

Formatted: English (United States)

Formatted: English (United States)

1 Zhang, Y., Carey, S.K., and Quinton, W.L.: Evaluation of the algorithms and parameterizations for ground
2 thawing and freezing simulation in permafrost regions. *J. Geophys. Res.*, 113, D17116, DOI:
3 10.1029/2007JD009343, 2008.

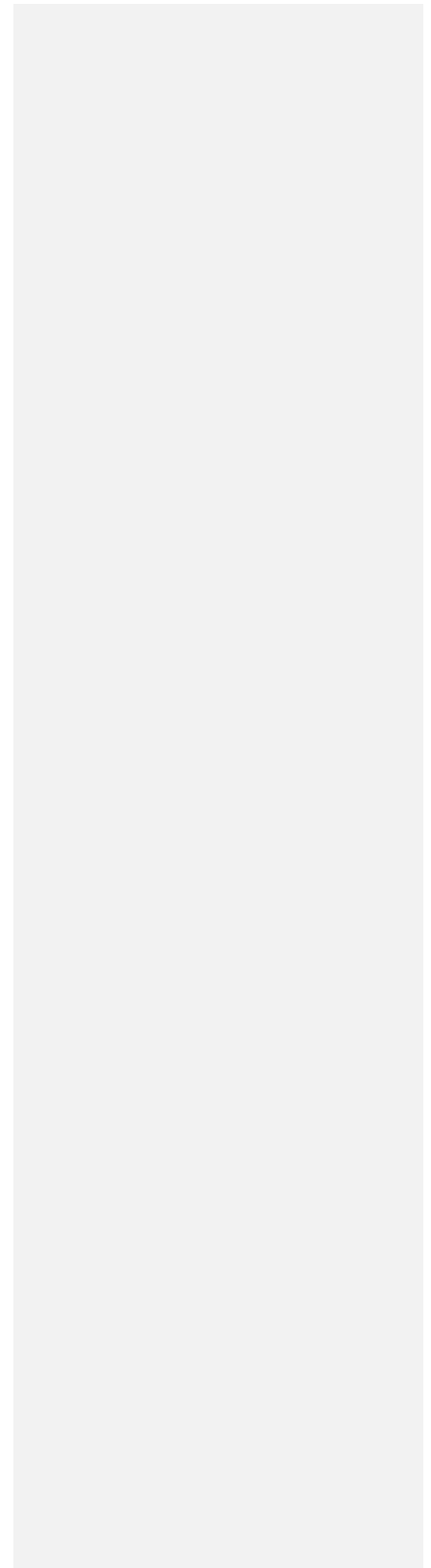
4 [Zhang, Y., Chen, W., and Rjseborough, D.: Temporal and spatial changes of permafrost in Canada since](#)
5 [the end of the Little Ice Age. *J. Geophys. Res.*, 111, doi:10.1029/2006JD007284, 2006.](#)

6

Formatted: English (United States)

1 Table 1. Variable values applied in the Stefan equation.

Variables		
thermal conductivity (k_{mw})	1.7	$\text{W m}^{-1} \text{K}^{-1}$
dry density of soil (ρ_m)	1600	kg m^{-3}
latent heat of fusion (L)	334	kJ kg^{-1}
total moisture content (W)	0.3	-
unfrozen water content (W_u)	0	-

2
3

- 1 Table 2. Calculated maximum annual active layer thickness using both the Stefan Equation and the
2 VAMPER model under different forcing scenarios.

Model Run	Average Annual Ground Surface Temperature	Annual Amplitude	Stefan Equation Active Layer	Vamper Model Active Layer
	(°C)	(°C)	(m)	(m)
1	-6	10	0.7	0.7
2	-4	10	1.0	1.0
3	-2	10	1.2	1.3
5	-6	20	1.6	1.7
6	-4	20	1.7	1.9
7	-2	20	1.9	1.9

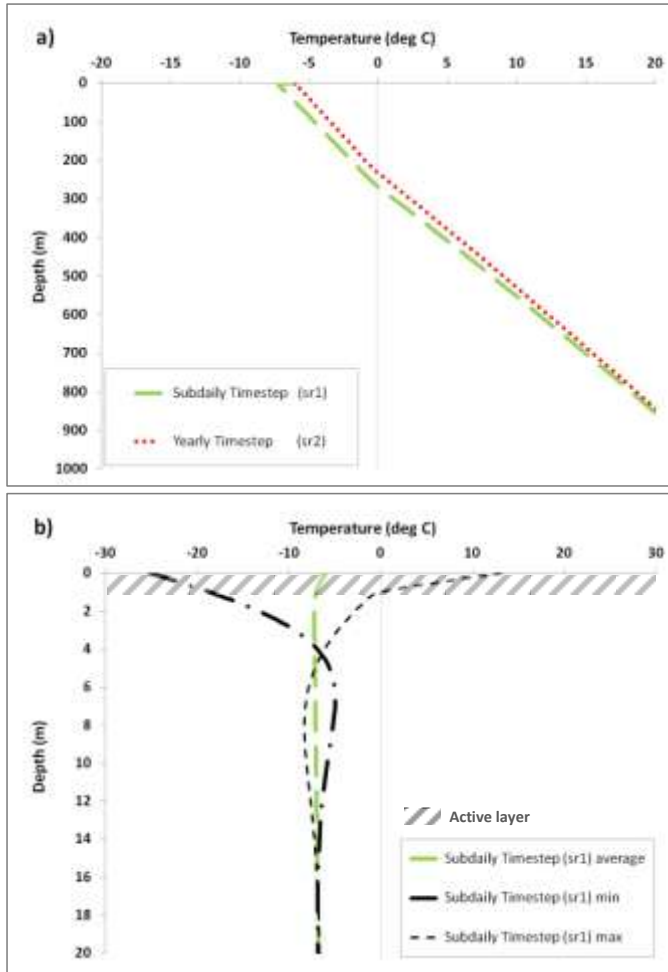
- 3
4
5
6

1 Table 3. The original lithological classification from Hartmann and Moosdorf (2012) and the
 2 reclassification scheme used for the ECBilt grid.

3

	Original Litho Class	VAMPER Class
1	Unconsolidated Sediments (SU)	Sed
2	Basic Volcanic Rocks (VB)	Bed
3	Siliciclastic Sedimentary Rocks (SS)	Sed
4	Basic Plutonic Rocks (PB)	Bed
5	Mixed Sedimentary Rocks (SM)	Sed
6	Carbonate Sedimentary Rocks (SC)	Sed
7	Acid Volcanic Rocks (VA)	Bed
8	Metamorphic Rocks (MT)	Bed
9	Acid Plutonic Rocks (PA)	Bed
10	Intermediate Volcanic Rocks (VI)	Bed
11	Water Bodies (WB)	N/A
13	Pyroclastics (PY)	Bed
12	Intermediate Plutonic Rocks (PI)	Bed
15	Evaporites (EV)	Sed
14	No Data (ND)	N/A
16	Ice and Glaciers (IG)	N/A

4



1

2

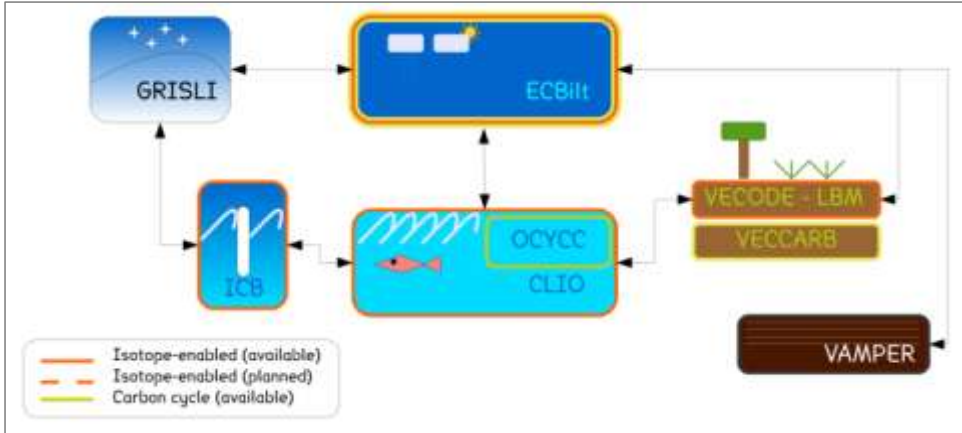
3

4 Figure 1. a) Plot comparing VAMPER model results using different timesteps (annual vs. sub-daily) but the

5 same annual average temperature forcing of -6°C . b) Plot showing the sr1 average, min, and max6 temperature-depth profiles. Also shown in b) is the ~ 1 m active layer, marked as diagonal lines.

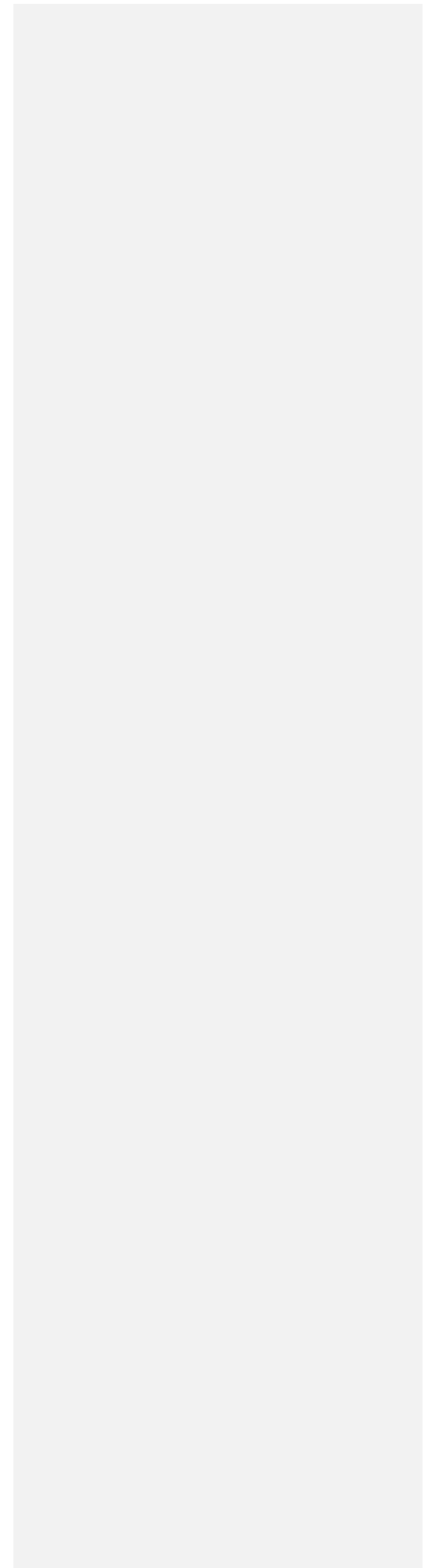
7

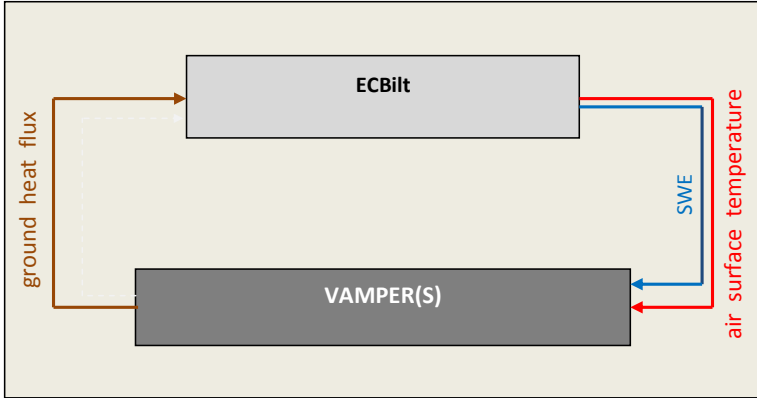
8



1
2
3

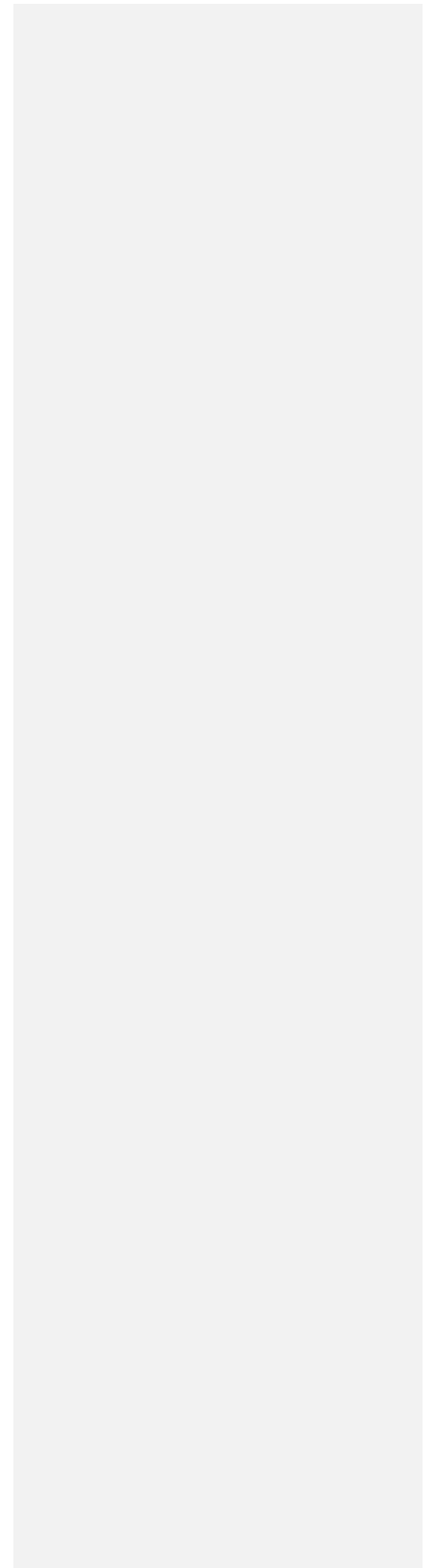
Figure 2. iLOVECLIM model component setup.

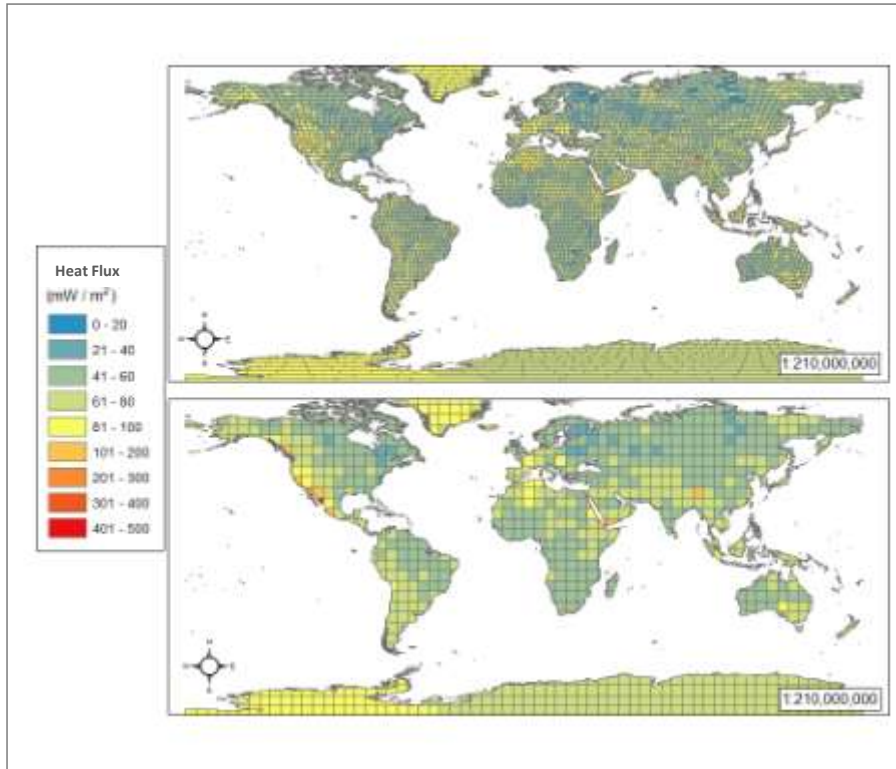




1
2
3
4
5

Figure 3. Coupling scheme between ECBit and the VAMPER(S) model showing the variables (air surface temperature, swe, and ground heat flux) passed between the components at each timestep.

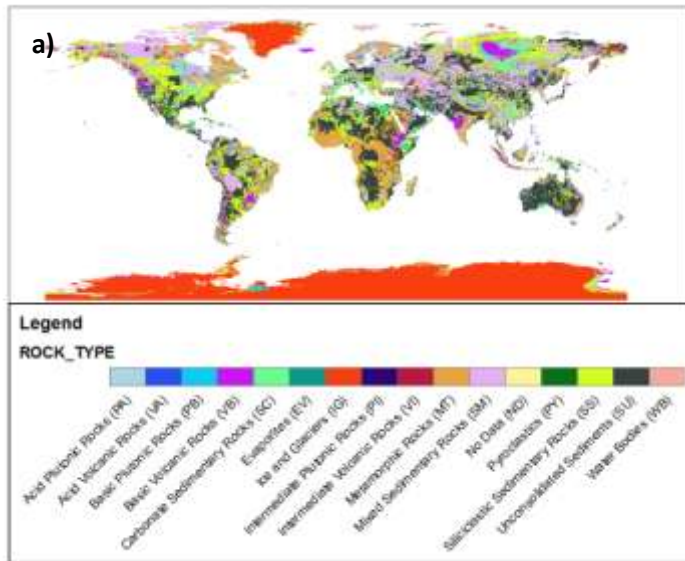




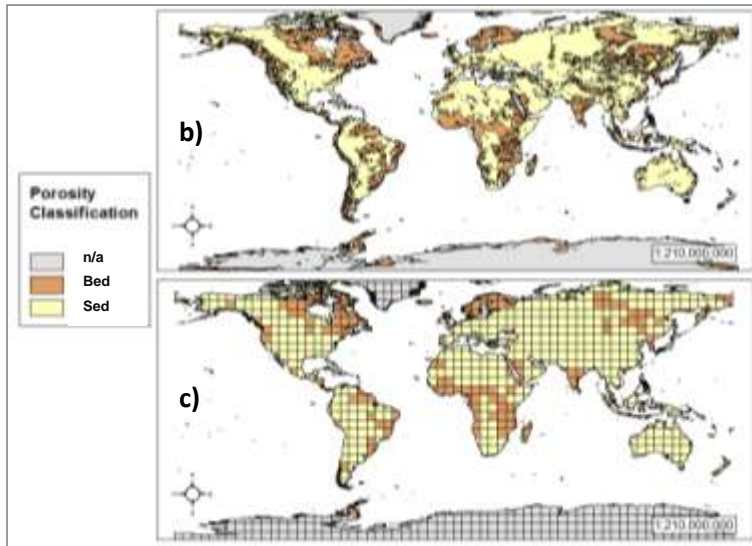
1
2

3 Figure 4. The original geothermal heat flux map (top) from Davies (2013) and the weighted average
4 version (top) for use as the lower boundary value in the iLOVECLIM experiments (bottom).

5



1

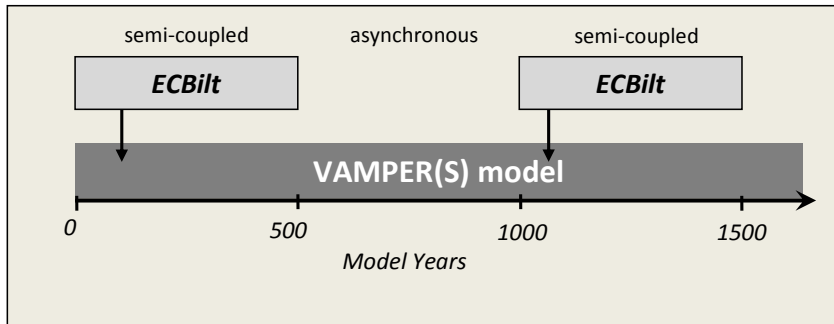


2

3

4 Figure 5. World maps showing a) original map from Hartmann and Moosdorf (2012) b) map of
 5 reclassified lithology using Table 2 and c) the version geo-processed to match the ECBilt grid resolution.

6

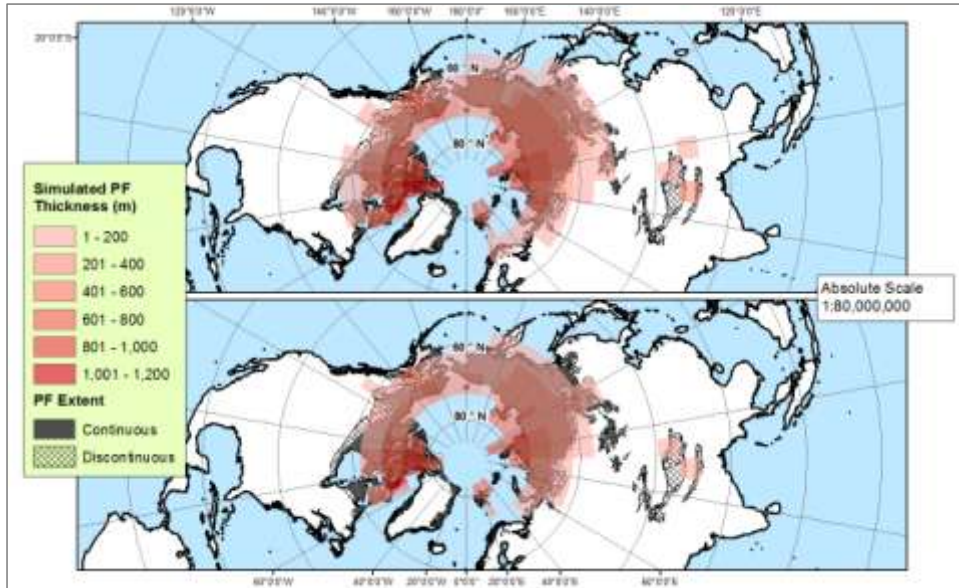


1

2

3 Figure 6. An illustration of asynchronous coupling between VAMPER(S) and ECBilt. The components are
4 run semi-coupled for 100 years while VAMPER(S) is run the entire time. This allows VAMPER(S) to
5 equilibrate with the climate state of *i*LOVECLIM using less computer resources time than a synchronous
6 version.

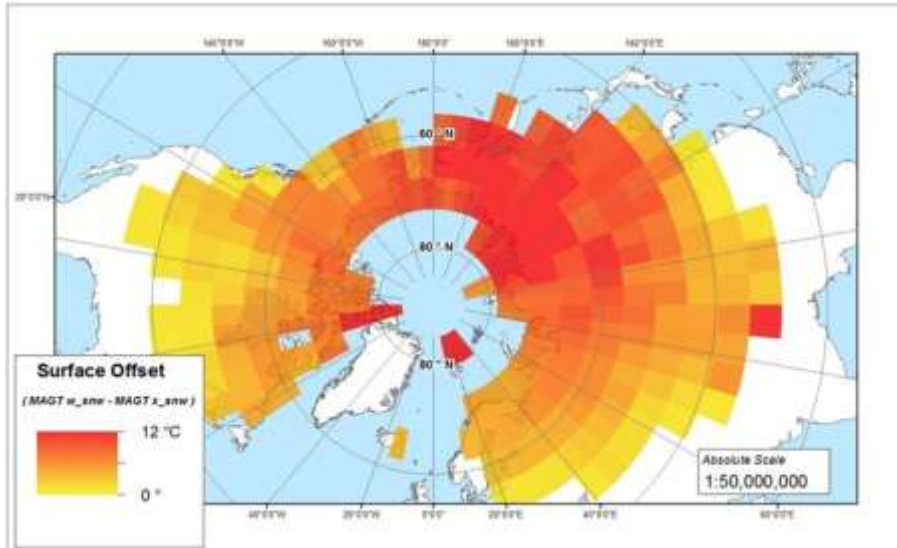
7



1
2

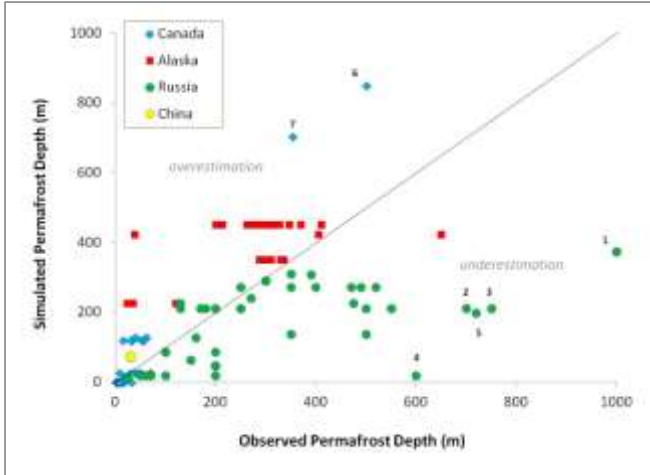
3 Figure 7. Preindustrial simulation results for permafrost thickness distribution using ECBILT-VAMPER
4 semi-coupling (top) and ECBILT-VAMPER_S semi-coupling (bottom).

5



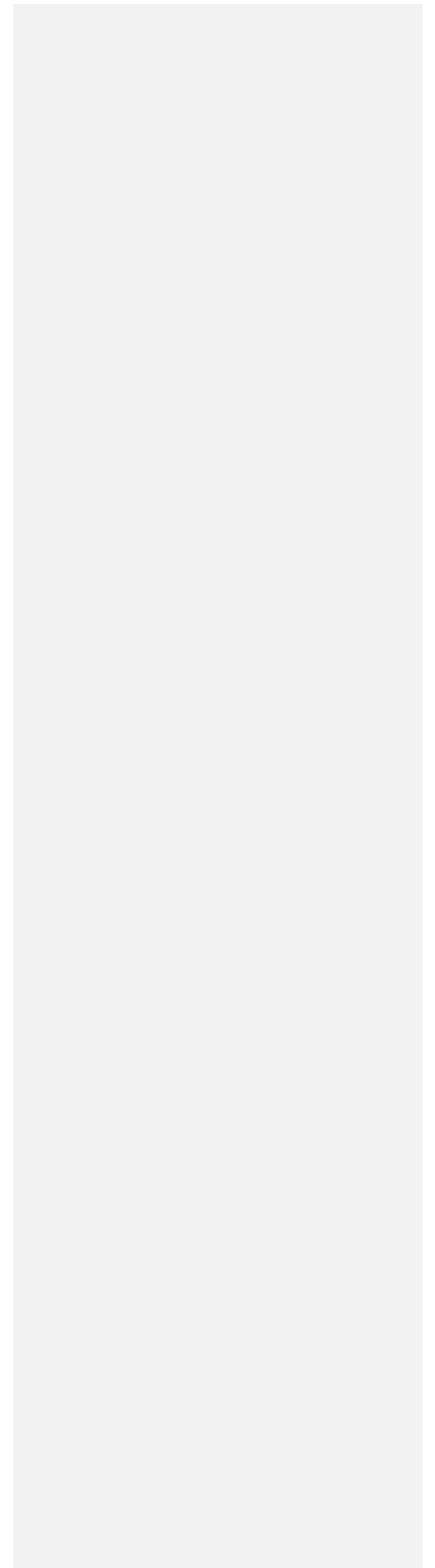
1
2
3
4
5

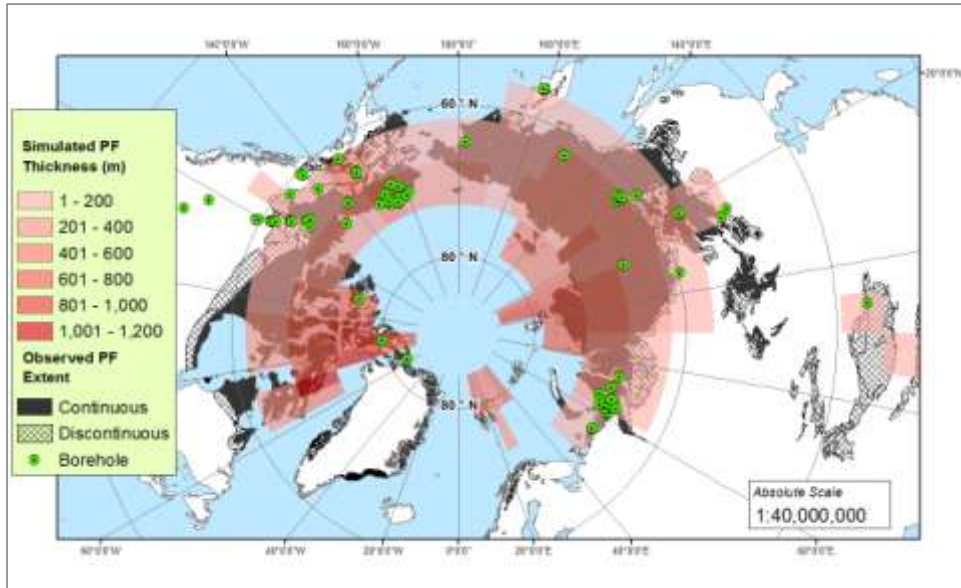
Figure 8. Mean annual surface offset as a result of including the snow [enhancement option](#) in the ECBilt-VAMPERS coupling.



1
2
3
4
5

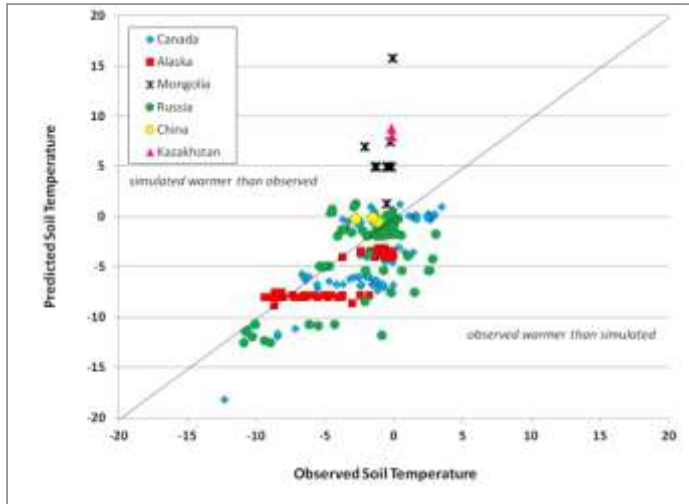
Figure 9. A 1:1 scatterplot comparing simulated thickness results with corresponding permafrost thickness estimates from borehole data. Points 1-7 are outliers mentioned specifically above.





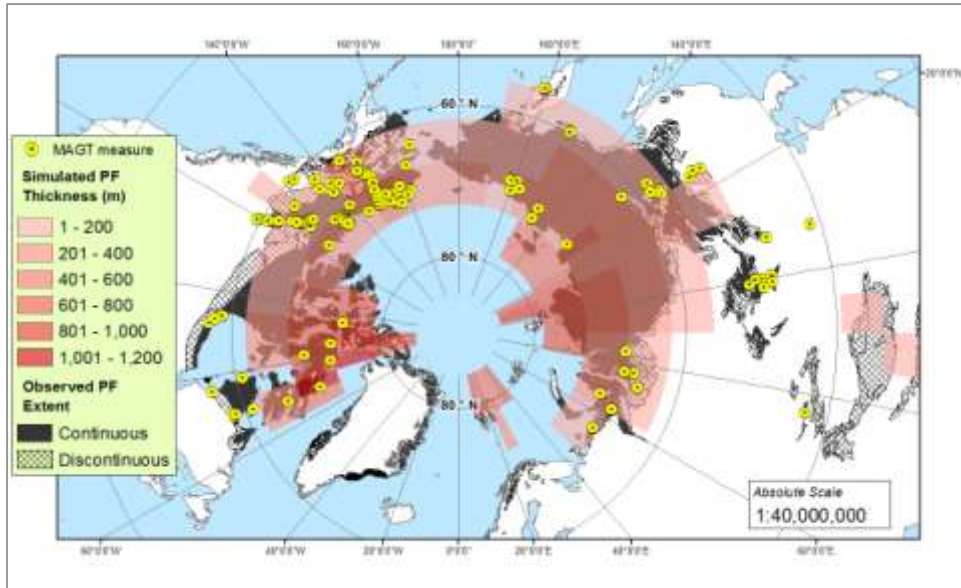
1
2
3
4
5
6

Figure 10. Map of deep GTN-P borehole locations with the simulated permafrost thickness (with snow enhancement) and observed PF extent (Brown et al., 2014).



1
2
3
4
5
6

Figure 11. A 1:1 scatterplot comparing simulated mean annual temperatures with corresponding MAGT measurements.



1
2
3
4
5

Figure 12. Map showing locations of the MAGT measurements, collected for the IPY 2010 (GTN-P), used in the comparison to corresponding *i*LOVECLIM simulated subsurface temperatures.